24th Annual Produced Water Seminar
January 14-16, 2014
The Nassau Bay Hilton, 3000 NASA Road One, Houston Texas 77058

CFD Analysis of Internal Flow Structures within a Class of Hydrocyclones

Abdul Motin[1], Presenter
André Bénard[1]; Charles A. Petty[2]; and, Volodymyr V. Tarabara[3]

[1]Mechanical Engineering; [2]Chemical Engineering & Materials Science; and,
[3]Civil & Environmental Engineering

Michigan State University, East Lansing, MI 48824, USA

Corresponding Author: Abdul Motin, motinabd@msu.edu

Summary

This paper uses computational fluid dynamic methods to examine the internal flows within a class of hydrocyclones used to clean produced water on offshore platforms. The separation performance of these hydrocyclones is sensitive to internal secondary flow structures, which may hydraulically block the overflow nozzle and, thereby, cause a precipitous and unexpected decline in the separation efficiency.

Introduction

Produced water is a multiphase fluid produced by a three-phase separator during the production of oil and gas. The concentration of the dispersed phase may be as large as 3,000 ppm of oil in water; the density difference between the dispersed phase and the continuous phase may be 0.10 g/cc or less; and, the domain of the particle size distribution of the dispersed phase may range from submicron to 50 microns due to process conditions upstream of the produced water treatment facility.

Current environmental regulations in the Gulf of Mexico require that the effluent underflow dispersion concentration be less than 30 ppm of an oil/grease phase as measured by a mandated standardized extraction procedure. Therefore, if the feed concentration of oil is 3,000 ppm, then the underflow purity coefficient, defined as

$$\varepsilon_U \equiv \frac{C_F - C_U}{C_F} \quad , \quad 0 \le \varepsilon \le 1 , \tag{1}$$

must be larger than 0.99 (i.e., $0.99 < \varepsilon < 1.00$) for the water treatment facility. In the above expression, C_F and C_U represent, respectively, the feed and underflow concentration of the dispersed organic phase. Presently, several different unit operations based on different physical principles are combined in parallel and series to insure that the effluent concentration of the produced water separation system complies with the discharge requirements. The focus of this

presentation is limited to the underlying physics of a single hydrocyclone separator and its contribution towards cleaning produced water.

Figure 1 shows how the purity coefficient of a single-stage, four-in-one hydrocyclone separator on an offshore platform in the North Sea depends on the volumetric feed flow rate with an overflow ratio in the range (see Meldrum, 1988):

$$0.01 < R_O \equiv \frac{Q_O}{Q_F} < 0.10 \,. \tag{2}$$

The flow rates Q_O and Q_F in Eq.(2) represent, respectively, the effluent rate of the overflow stream and the influent rate of the feed stream. The overflow ratio is small because the concentration of oil in the feed stream is small. If the feed stream to the four-in-one separator is equally distributed among the four hydrocyclones, then the offset on Figure 1 shows how the feed Reynolds number of a single hydrocyclone affects the purity coefficient over the range $25,000 < Re_F < 50,000$, where the feed Reynolds number is defined as

$$Re_F \equiv \frac{\rho_C U_F D_F}{\mu_C} \quad , \quad U_F \equiv \frac{(Q_{4F}/4)}{A_F} \quad , \quad \frac{\pi}{4} D_F^2 \equiv A_F \,. \tag{3}$$

In the above definition, ρ_C and μ_C represent the density and the viscosity of the continuous phase; Q_{4F} is the influent volumetric flow rate to the four-in-one separator; A_F is the cross sectional area of the feed inlet of an individual single-inlet hydrocyclone; U_F is the bulk average velocity of the feed stream within a single-inlet hydrocyclone; and, D_F is a characteristic diameter associated with the feed inlet. The individual hydrocyclones have a cylindrical swirl chamber of diameter $D_H (= 70\text{mm})$ and a frustoconical section containing two cones: an upper cone with a major diameter of 70 mm; and, a lower cone with a major diameter of 35mm. The length to diameter ratio of the deoiling hydrocyclone separator is relatively large ($L_H / D_H \cong 20$) compared with standard hydrocyclone technology ($L_H / D_H \cong 5$).

The results reported in Figure 1 show a catastrophic reduction in the underflow purity coefficient at a Reynolds number around 55,000. Meldrum (1988) conjectured that this upper bound on the capacity of a four-in-one single stage separator was related to a decrease in the core pressure of the individual hydrocyclones relative to the overflow plenum pressure. Figure 1 also shows that the underflow purity coefficient is insensitive to the Reynolds numbers between 25,000 and 50,000. The insensitivity of the separation performance to feed fluctuations is an attractive feature of hydrocyclone technology, which is still not fully understood.

It is noteworthy that the individual hydrocyclones used in the four-in-one separator stem from a multi-year discovery and development research program at the University of Southampton (UK) by M. Thew and his colleagues. For a lucid and insightful summary of the Colman/Thew hydrocyclone for deoiling dilute water solutions, see Thew (2000) as well as Hargreaves and Silvester (1990).

In order to treat a large amount of water exclusively by hydrocyclones, a separator system would clearly need many individual hydrocyclones in parallel followed by additional stages in series. This strategy would yield a high recovery of "clean" water (over 90% of the total influent feed) with an underflow purity coefficient that complies with local regulations. Clearly, a better understanding of the internal hydrodynamic phenomena that limits the turndown ratio and the cut-size of an individual hydrocyclone separator could lead to an improved compact separator system design that is reliable and simple to operate.

This paper examines the internal flow structure of a class of hydrocyclones developed by Young et al. (1994). Commercially available software (i.e., Fluent 6.6 supported by ANSYS 14.5, 2013) is used to solve the Reynolds averaged Navier-Stokes (RANS) equation and the Reynolds averaged continuity equation for a constant property Newtonian fluid. A transport equation (i.e., an equation-of-change for the Reynolds stress) is used to close the RANS-equation (see Pope, 2000). The cut-size of the separator at different Reynolds numbers for a fixed overflow ratio is determined by integrating the Reynolds averaged kinematic equation and force balance on an oil droplet.

Geometry and Operating Principles

In this study, computational fluid dynamic (CFD) methods were used to predict the mean velocity and pressure fields of a single phase Newtonian fluid with constant physical properties within a class of hydrocyclones defined by Figure 2. The model hydrocyclone has two symmetric rectangular channel inlets fitted tangentially to the swirl chamber near the overflow nozzle. The hydrocyclone has two effluent nozzles: an overflow cylindrical nozzle that removes the core flow; and, an underflow cylindrical nozzle that removes the sidewall boundary flow.

Unlike many standard hydrocyclone operations, a deoiling hydrocyclone operation places a significant backpressure on the overflow and the underflow withdrawal plena. This prevents the dissolution of dissolved gases and/or the entrainment of external gases into the core of the flow field. In the CFD simulations, the cross sectional average back pressure on the overflow nozzle is constant. The overflow ratio was 10% of the feed rate (i.e., $R_O = 0.10$ for all Reynolds numbers). This was accomplished by adjusting the cross sectional average back pressure on the underflow nozzle:

$$P_O \equiv \frac{\iint_{A_O} < \hat{p} > d\hat{A}_O}{A_O} = \text{constant}\,,\ \forall\, Re_F$$

$$P_U(Re_F) - P_O \equiv \frac{\iint_{A_O} < \hat{p} > d\hat{A}_U}{A_U} - \frac{\iint_{A_O} < \hat{p} > d\hat{A}_O}{A_O} \quad \ni \frac{Q_O}{Q_F} \cong 0.10 \qquad (4)$$

The simulations were performed for five different feed Reynolds number between 14,000 and 72,000. The feed Reynolds number is defined by Eq. (3) with U_F equal to the bulk average velocity in a single tangential inlet (see Figure 2), and with D_F equal to the equivalent diameter of the inlet.

In a vortex flow, a dispersed phase with a density less than the continuous phase will drift towards the low pressure region of the flow field (i.e., the core of the vortex). If Stokes' law holds, the radial component of the drift velocity of an oil droplet depends on the following factors: 1) the density difference between the two phases; 2) the radial component of the centrifugal acceleration; 3) the viscosity of the continuous phase; and, 4) the diameter of the dispersed particle. The following quasi steady-state balance equation gives an estimate for the radial component of the drift velocity:

$$\underline{e}_r \cdot [< \underline{u}_D > - < \underline{u}_C >] \equiv \underline{e}_r \cdot [< \underline{u}_{Drift} >] = \frac{(\rho_D - \rho_C)\ell_D^2}{18\mu_C} \frac{(\underline{e}_\theta \cdot < \underline{u}_D >)^2}{r} . \tag{5}$$

The position of an oil droplet in the flow field is determined by the following kinematic equation:

$$\left. \frac{\partial < \underline{\chi}_D > (\underline{X}_D, t)}{\partial t} \right|_{\underline{X}_D} = < \underline{u}_D > \quad , \quad < \underline{u}_D > = < \underline{u}_C > + < \underline{u}_{Drift} > \quad , \quad \underline{X}_D = < \underline{\chi}_D > (\underline{X}_D, 0) . \tag{6}$$

For each Reynolds number, Eq.(6) can be integrated for specific size particles starting at different positions on the influent feed plane. The particles can be tracked and will exit the confined vortex flow field by crossing either the effluent overflow nozzle or the effluent underflow nozzle. The ℓ_{50} cut-size of the separator is defined as the particle size for which 50% of the particles will report to the underflow and 50% of the particles will report to the overflow. The ℓ_{50} cut-size will depend on the following factors:

1) the maximum particle size, ℓ_{max};
2) the feed Reynolds number Re_F;
3) the overflow ratio R_O;
4) the shape of the hydrocyclone, and
5) the density ratio, $(\rho_D - \rho_C)/\rho_C$.

For statistically stationary conditions, the following macroscopic balance equation holds for the dispersed phase concentration with particle sizes between ℓ_D and $\ell_D + \Delta\ell_D$:

$$Q_F C_F f_F(\ell_D) d\ell_D = Q_O C_O f_O(\ell_D) d\ell_D + Q_U C_U f_U(\ell_D) d\ell_D . \tag{7}$$

The above equation assumes that there is no coalescence or breakup of droplets within the hydrocyclone. The term $f_X(\ell_D)d\ell_D$ represents the volume fraction of the dispersed phase with sizes between ℓ_D and $\ell_D + \Delta\ell_D$ and the integral of Eq.(7) over all sizes yields the following steady-state equation for the dispersed phase:

$$Q_F C_F = Q_O C_O + Q_U C_U . \tag{8}$$

For dilute mixtures, the volumetric flow rates are approximately balanced:

$$Q_F \cong Q_O + Q_U . \tag{9}$$

The overflow grade efficiency, $G_O(\ell_D;\ell_{max})$, of a separator is defined as the fraction of the dispersed phase that reports to the overflow stream. The overflow grade efficiency is related to the size distributions of the overflow and the feed streams as follows:

$$G_O(\ell_D;\ell_{max})Q_F C_F f_F(\ell_D)d\ell_D = Q_O C_O f_O(\ell_D)d\ell_D . \tag{10}$$

An integral of Eq.(10) over all sizes yields the following relationship between the overflow grade efficiency, the particle size distribution of the feed stream, and the recovery coefficient E_O :

$$\frac{Q_O C_O}{Q_F C_F} \equiv E_O = \int_0^{\ell_{max}} G_0(\ell_D) f_F(\ell_D) d\ell_D . \tag{11}$$

Equations (8) and (9) imply that the underflow purity coefficient, ε_U, is related to the overflow recovery coefficient, E_O, and the overflow split ratio, R_O, as follows

$$\varepsilon_U = \frac{E_O - R_O}{1 - R_O} . \tag{12}$$

This relationship motivates the use of the reduced grade efficiency:

$$\tilde{G}_O(\ell_D;\ell_{max}) \equiv \frac{G_O(\ell_D;\ell_{max}) - R_O}{1 - R_O} . \tag{13}$$

It is noteworthy that the integral of Eq.(13) over all particle sizes yields the following relationship between the underflow purity coefficient, the particle size distribution in the feed stream, and the reduced grade efficiency of the hydrocyclone:

$$\int_0^{\ell_{max}} \tilde{G}_0(\ell_D;\ell_{max}) f_F(\ell_D) d\ell_D = \varepsilon_U \equiv \frac{C_F - C_U}{C_F} . \tag{14}$$

The reduced grade efficiency will depend on the feed Reynolds, the overflow ratio, the density ratio, and the shape of the hydrocyclone.

Results and Discussion

Figure 3 shows that for a constant overflow ratio, the aspect ratio of the vortex core (i.e., L_C / D_H) increases as the feed Reynolds number increases, but decreases for $Re_F > 21,408$. This result supports the idea that the core flow blocks the passage of fluid into the effluent nozzle at large Reynolds numbers.

For a feed Reynolds number of 29,735, Figure 4 shows the velocity vector field projected onto the A-B plane defined by Figure 2. The simulation indicates that an inward flowing boundary layer (see region R1) is balanced by a radial pressure drop imposed on the end wall. This short circuit flow from the feed inlet to the effluent nozzle is called an Ekman boundary layer. It is noteworthy that a toroidal recirculation zone (see region R3) forms between the vortex core and the outer flow field. An additional recirculation zone (see region R2) develops near the top wall of the inlet chamber.

Figure 5a divides the flow field within the swirl chamber into three zones. The contribution from each zone to the effluent overflow rate is quantified by Figure 5b for a range of feed Reynolds numbers. The effluent overflow rate is equal to the algebraic sum of the radial inflow from the three zones and the reverse flow from the downstream.

Figure 5b shows that the radial inflow through the boundary B1 is the largest among the three zones. The inflow through the boundary B1 has a negligible tangential component as well as a short residence time. Consequently, this region would not contribute to the separation of the dispersed phase. It is noteworthy that as the feed Reynolds number increases, Q1 first decreases and then increases; as the feed Reynolds number continues to increase, Q1 decreases again.

For low feed Reynolds numbers, the swirl component of the velocity field and the aspect ratio of the vortex core are small (see Figure 3). As a consequence, the reverse flow in the core is accommodated by the vortex finder and there is no inward or outward flow through the boundary B2. However, with an increase in the Reynolds number, the swirl component increases and a larger axial flow from this region cannot be accommodated by the effluent nozzle. As a result, part of the reverse flow in the outer periphery of the vortex core moves outward through B2. For $Re_F < 30,000$, Zone 3 shows a radial outflow through the boundary B3. For all other Reynolds numbers, there is a radial inflow through the boundary B3, which indicates a short circuit flow from the inlet to the vortex core through B3. This radial inward flow through B3 possesses less residence time, which would yield a reduction in the separation of an oil-water mixture

Figure 6 shows the influence of the feed Reynolds number on the aspect ratio of the core flow, L_C / D_H and the normalized cut-size of the separator, $\ell_{50} / (\ell_{50})_{min}$. The maximum aspect ratio of the core is about 4.5 times the diameter of the swirl chamber. This length decreases with an increase in the Reynolds number. The cut-size of the hydrocyclone decreases with an increase in the feed Reynolds number up to 30,000 and then increases. The radial outflow through B2 and B3 for a feed Reynolds number of 21,408 and 29,735 restricts the short circuit flow from the inlet to the vortex core and, thereby, increases the residence time of a dispersed droplet (see Figure 4 and Figure 5). The larger aspect ratio of the core region for these Reynolds numbers decreases the cut-size. However, even though the tangential component of the velocity

field increases with an increase in the feed Reynolds number, the radial inflow through B1, B2 and B3 together with the smaller core at feed Reynolds numbers larger than 30,000 cause the cut-size to increase.

Salient Conclusions

The aspect ratio of the core flow near the entry to the effluent nozzle decreases with an increase in the feed Reynolds number. This phenomenon coincides with the onset of a toroidal recirculation zone inasmuch as the effluent overflow nozzle cannot accommodate an increase in flow from the core. As a consequence, the residence time of a dispersed droplet increases, which yields a lower cut-size. The higher radial inflow through the B1 and B2 for feed Reynolds numbers less than 30,000 supports a short circuit flow from the inlet to the core.

Acknowledgement

Support for this research from the United States Environmental Protection Agency (RC-83518301), NSF Partnership of International Research and Education (???), and SPG (what's this?) are gratefully acknowledged.

References

ANSYS, 2013. Fluent documentation: Theory guide.

Hargreaves, J. and R. Silvester,1990, Computational fluid dynamics applied to the analysis of deoiling hydrocyclone performance, Chem. Eng. Res. Des., Vol. 68(4), 365-383.

Meldrum, N., 1988. Hydrocyclones: A solution to produced water treatment. SPE Product. Eng. 3(4), 669-676.

Pope, S.B., 2000. Turbulent flow, Cambridge Univ. Press, Cambridge, England.

Thew, M., 2000, Cyclones for oil/water separation, in Wilson, I.D. (Ed.), Encyclopedia of Separation Science, Vol. 4, 1480–1490, Academic Press.

Young, G., W. Wakley, D. Taggart, S. Andrews, J. Worrell, 1994, Oil-water separation using hydrocyclones: an experimental search for optimum dimensions, J. Petrol. Sci. Eng., Vol. 11, 37-50.

Appendix

List of Notations

Symbols	Description	Unit
A	Area	m^2
C	Concentration	ppm
D	Diameter of swirl chamber	m
d_{50}	Cut size	m
E	Recovery coefficient	-
G	Grade efficiency	-
L	Length of the hydrocyclone	m
Lc	Reverse flow core length	m
ℓ	Length scale of droplets	m
P	Pressure	Pa
Q	Flow rate	m3/s
R	Flow ratio	-
Re	Reynolds number	-
U	Velocity	m/s
u	Fluctuating velocity	m/s
ε	Purity coefficient	-
μ	Viscosity	Pa-s
ρ	Density	kg/m^3

Subscripts

C	Continuous phase
D	Dispersed Phase
F	Feed
H	Hydrocyclone
O	Overflow
U	Underflow

List Figures

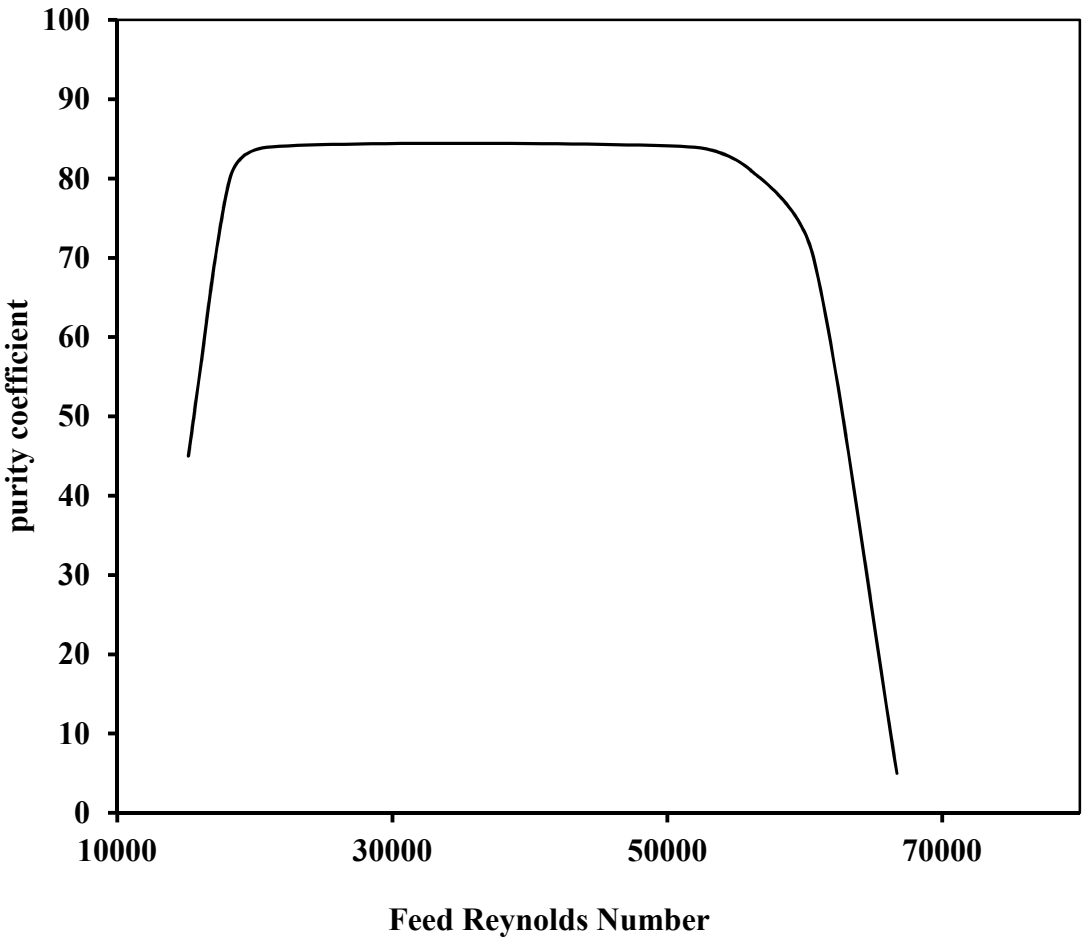
100
90
80
70
60
50
40
30
20
10
0
purity coefficient
10000
30000
50000
70000
Feed Reynolds Number

Figure 1

D (mm)	Do/D	Du/D	D_F/D	Lc/D	L/D	Lv/D	Lu/D	θ
26	0.07	0.23	0.275	1	7.37	0.1	9.71	6^0

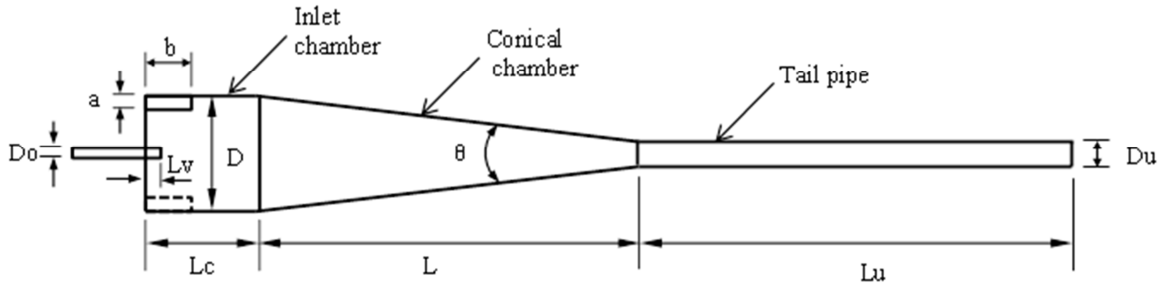

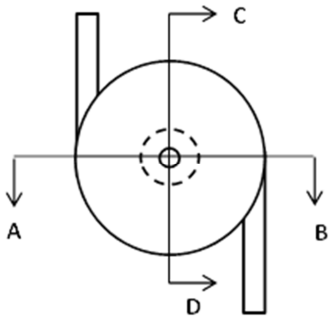

Figure 2

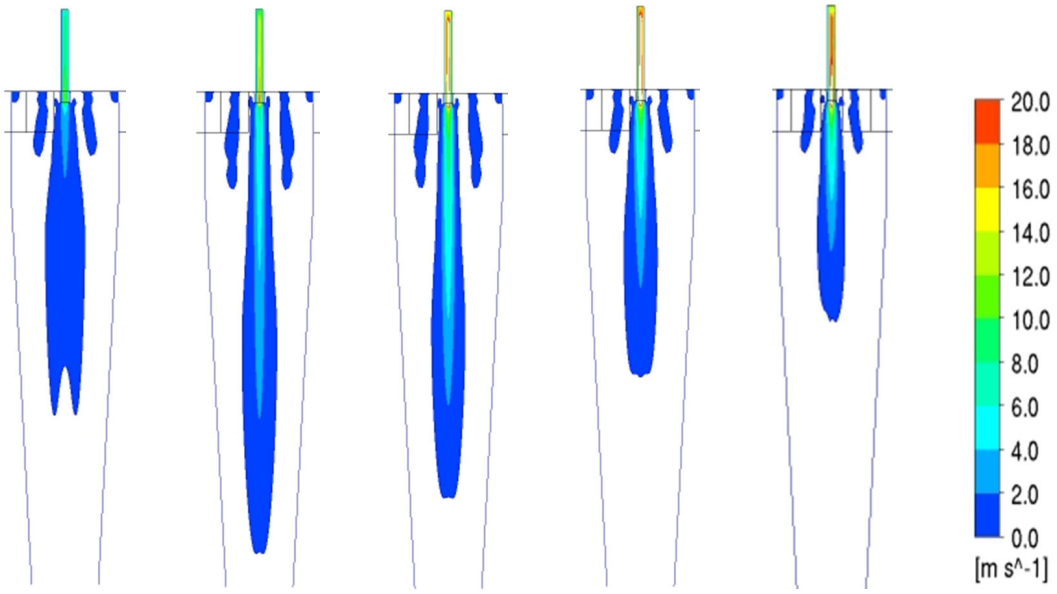

Re = 14272 Re = 21408 Re = 29735 Re = 35680 Re = 71360

Figure 3

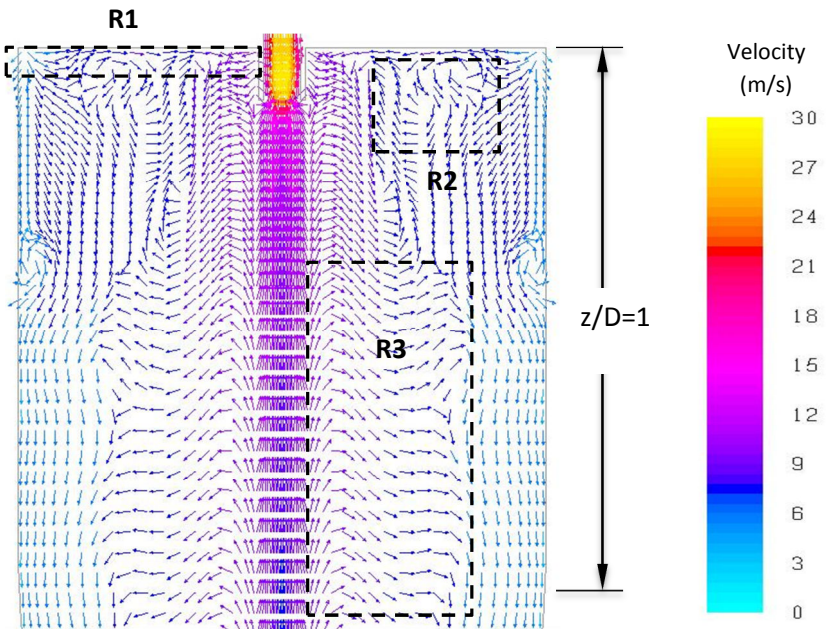

Figure 4

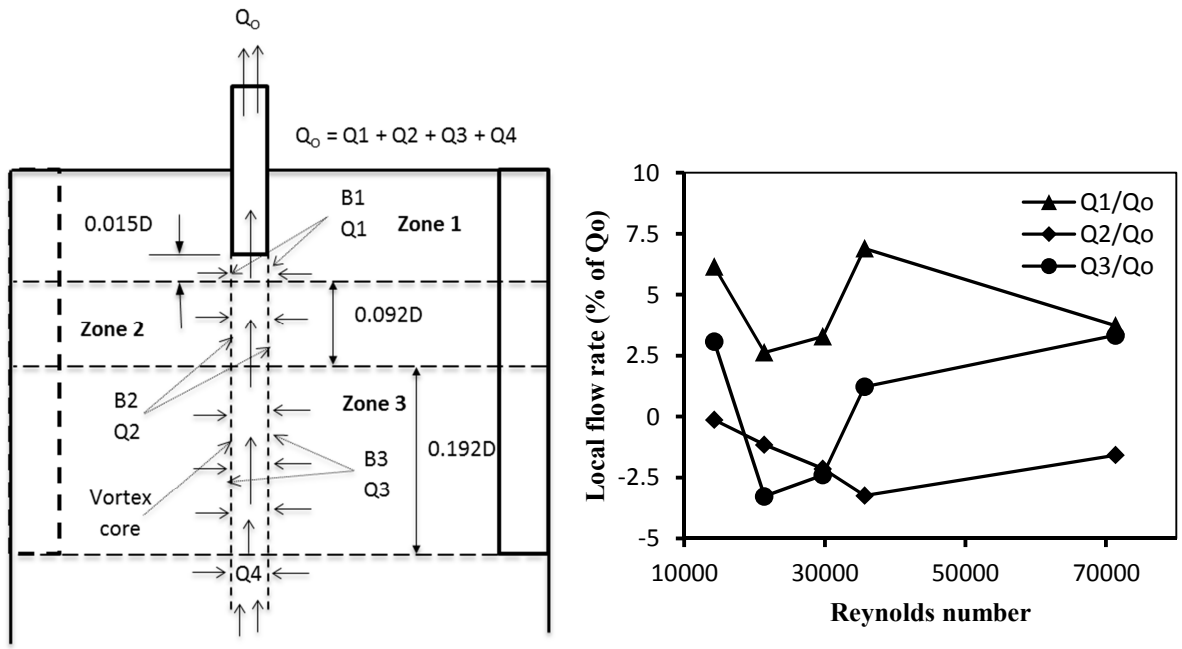
Qo
Qo = Q1 + Q2 + Q3 + Q4
0.015D
B1
Q1
Zone 1
Zone 2
0.092D
B2
Q2
Zone 3
0.192D
B3
Q3
Vortex
core
Q4
Local flow rate (% of Qo)
10
7.5
5
2.5
0
-2.5
-5
10000
30000
50000
70000
Reynolds number
Q1/Qo
Q2/Qo
Q3/Qo

(a) (b)

Figure 5

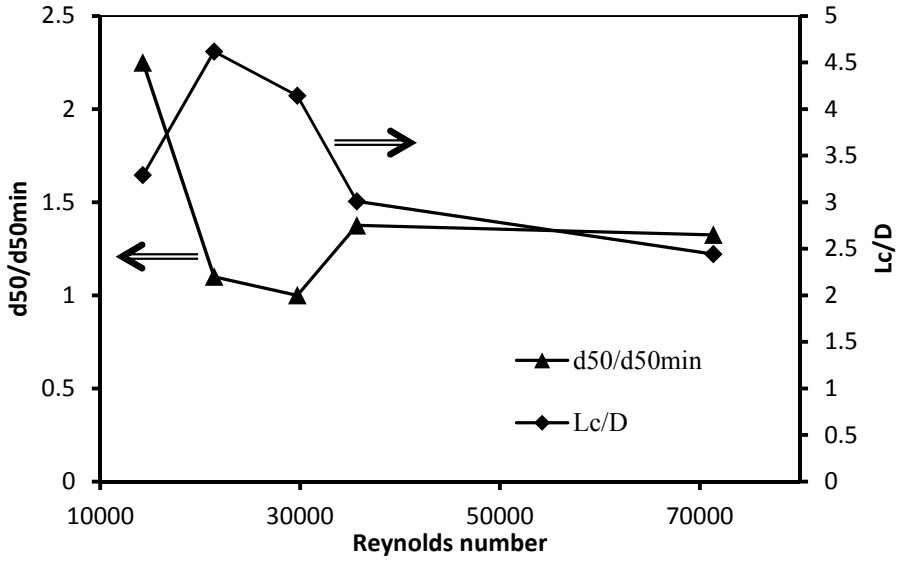
2.5
2
1.5
1
0.5
0
d50/d50min
5
4.5
4
3.5
3
2.5
2
1.5
1
0.5
0
Lc/D
10000
30000
50000
70000
Reynolds number
d50/d50min
Lc/D

Figure 6